Journal of Manufacturing Processes 93 (2023) 260–274

Contents lists available at ScienceDirect

Journal of Manufacturing Processes

journal homepage: www.elsevier.com/locate/manpro

Improvement of tensile and flexural properties of 3D printed PEEK through the increase of interfacial adhesion

Pedro Rendas [a,*], Lígia Figueiredo [b], Madalena Geraldo [a], Catarina Vidal [a,c], B.A. Soares [a,c,**]

[a] Department of Mechanical and Industrial Engineering, UNIDEMI, NOVA School of Science and Technology, Universidade Nova de Lisboa, 2829-516 Caparica, Portugal
[b] Bioceramed - Cerâmicos para Aplicações Médicas S.A., São Julião do Tojal 2660-360, Portugal
[c] Laboratório Associado de Sistemas Inteligentes, LASI, 4800-058 Guimarães, Portugal

ARTICLE INFO

Keywords:
Polyetheretherketone
PEEK
Fused Filament Fabrication
Additive Manufacturing
Mechanical properties

ABSTRACT

Polyetheretherketone (PEEK) is the leading high-performance biocompatible thermoplastic for the replacement of metals in orthopaedic applications. PEEK processing using material extrusion (ME) Additive Manufacturing (AM) techniques such as Fused Filament Fabrication (FFF) highlight its potential for the manufacture of patient-specific load-bearing implantable medical devices. As a high temperature semi-crystalline polymer, the mechanical properties of PEEK 3D printed samples are significantly influenced by printing parameters, particularly the crystallinity and interfacial adhesion of 3D printed parts. Given these challenges, the printing parameters of nozzle temperature, zone heater temperature, layer height and extruder multiplier were selected and studied for their effects in the interfacial adhesion and thus consequent mechanical performance of PEEK 3D prints. Design of Experiment (DoE) studies were conducted where the Taguchi and ANOVA analysis were used to determine the optimal parameter combinations and respective contributions. Additionally, different infill configurations were used with the optimal parameters to lower the samples' void volume and increase interface bonding. Reductions of up to 65 % in void volume were obtained with an interlayer translation of the infill lines and the tested configurations yielded improvements in both the tensile and flexural properties of 3D printed PEEK. Furthermore, high-temperature annealing treatments produced further increases in the strength, stiffness and crystallinity of PEEK samples. With this, significant improvements in both the void volume and the tensile and flexural properties of PEEK prints were achieved in support of the use of 3D printed PEEK in the manufacture of custom-made and high performance implantable medical devices.

1. Introduction

Additive Manufacturing (AM) techniques, commonly referred to as three-dimensional (3D) printing, have become increasingly relevant for their ability to produce unique complex geometries with less material waste in comparison to conventional subtractive manufacturing techniques [1]. AM consists of layer-by-layer deposition of material corresponding to cross-sections of virtual 3D models based in Computer-Aided Design (CAD). This makes AM flexible to design changes and makes this manufacturing technology very attractive to industries where products need to be customized to the end-user. For these reasons, AM has become particularly attractive in the medical field where AM-compatible biomaterials can be used to produce patient-specific medical devices based on medical imaging data or to manufacture complex 3D scaffold structures for tissue engineering [2,3].

Among AM-compatible biomaterials, Polyetheretherketone (PEEK) has stood out as the leading high-performance thermoplastic material for orthopaedic, trauma and spinal medical applications due to its high strength-to-weight ratio and chemical stability which make it biocompatible and resistant to *in vivo* degradation [4,5]. Furthermore, PEEK's rigidity is closer to that of human bone which allows for a more effective implant-bone load transfer whereas more rigid metal materials, such as titanium, could cause stress shielding of the treated bone and lead to bone resorption [6]. As a thermoplastic material, PEEK is compatible with Material Extrusion (ME) Additive Manufacturing (AM) techniques such as Fused Deposition Modelling (FDM®, Stratasys, USA), which is

* Corresponding author.
** Correspondence to: B.A. Soares, Department of Mechanical and Industrial Engineering, UNIDEMI, NOVA School of Science and Technology, Universidade Nova de Lisboa, 2829-516 Caparica, Portugal.
E-mail addresses: p.rendas@campus.fct.unl.pt (P. Rendas), ba.soares@fct.unl.pt (B.A. Soares).

https://doi.org/10.1016/j.jmapro.2023.03.024
Received 28 November 2022; Received in revised form 14 March 2023; Accepted 18 March 2023
Available online 27 March 2023

also referred to as Fused Filament Fabrication (FFF). This makes 3D printed PEEK highly suitable for the manufacture of patient-specific load-bearing implantable medical devices. One example of such applications is the high-temperature laser sintering (HT-LS) of PEEK cranial plates as studied by Berretta, Evans and Ghita [7]. Additionally, the combination of high-performance materials such as PEEK with 3D printing techniques enables customization of the implant not only towards the patient but also towards its functionalization. Here, 3D printed scaffolds and porous structures can improve certain biofunctionalities like the increase of osseointegration in orthopaedic implant applications [8].

Besides customization, AM also allows the variation of process parameters throughout the print. Interesting research has showed that it is possible to increase the structural integrity of printed parts with real-time parameter adjustment [9]. Furthermore, a similar multi-parameter approach can be combined with numerical simulation to strengthen specific areas of a print depending on the type of loads identified. This highlights the need to study the effects of 3D printing parameters for all load conditions.

Still, the use of PEEK's material extrusion AM for load-bearing applications like the manufacture of orthopaedic implants can be challenging which sparked research in the improvement of the mechanical performance and bioactivation of 3D printed PEEK [10]. Concerning its mechanical performance, PEEK's semi-crystalline nature means that its mechanical behaviour is influenced by its crystalline content, which may vary depending on the thermal processing conditions of the manufacturing process. For this, slower cooling rates were found to produce PEEK samples with a higher percentage of the crystalline phase [11] which can correspond to samples with higher strength and fracture toughness [12]. Furthermore, heat treatments can be used to increase this crystalline phase and improve the mechanical performance of PEEK samples. Annealing treatments with slow heating/cooling rates and longer times at maximum temperature have been shown to increase PEEK samples strength and stiffness [13,14].

The mechanical properties of 3D printed components are also significantly influenced by FFF parameters. The effects of some of these parameters seem to be well established. The correct choice of build orientation has been shown to significantly increase the tensile, flexural and compressive properties for PEEK samples that were printed with lines deposited parallel to the loads [15,16]. The weaker interfaces created between lines and layers where the filament bonded make 3D components anisotropic and thus, loads carried axially through the lines and longitudinally through the layers will be supported better than those causing shear were the filament bonded [17–20]. Infill percentage, in turn, is directly related to the amount of material supporting the load. Higher infill percentages correspond to larger effective cross-section areas for load support and increase the samples strength and rigidity. Both build orientation and infill percentage were found to have a significant impact in the mechanical behaviour of PEEK samples where the brittle fracture transitioned to ductile fracture after yield and increased strength for samples with maximum infill percentage and build orientation aligned with the loads [21].

Apart from this, the mechanical performance of 3D printed PEEK samples with 100 % infill and equivalent build orientation can vary depending on the filament bonding conditions. FFF parameters such as printing temperatures are related to the polymer chain mobility required for fusion and influence the material's fluidity upon deposition [22,23]. In PEEK's case, ambient temperature can be especially relevant due to its high printing temperatures. Besides reducing cooldown rates and consequent warping defects, higher ambient temperatures can improve bonding conditions and have been shown to result in PEEK samples with higher tensile strength and modulus [14,24]. Nozzle temperatures are related to the material's viscosity and higher temperatures can increase adhesion not only through increased molecular mobility but also through larger adhesion surfaces as lower viscosity can result in more material spread upon deposition [25]. For these reasons, both the density and the tensile strength of PEEK samples was reported to increase with nozzle temperature [26]. However, excessive nozzle temperature can also increase warping and result in polymer degradation [24].

Other printing parameters can influence the area of contact between deposited lines and layers and thus improve the interfacial adhesion of 3D prints. As the nozzle is an important heat source for filament bonding, higher printing speeds can lower flow stability and increase cooldown rates which worsens interfacial adhesion and results in lower tensile strength and higher void contents [26]. The void contents of a PEEK print can be reduced by improving flow stability using screw extrusion-based FFF equipment [27], however, the void contents of 3D printed components are typical of FFF deposition and are largely unavoidable. The void contents of PEEK 3D prints have been reported to account for as much as 8 % in volume even for 100 % infill samples [21].

For PEEK 3D printing, the void contents can be an especially significant issue due to PEEK's high notch sensitivity [28]. PEEK's fatigue life was shown to be spent mostly on crack nucleation and once the crack initiates, crack propagation rates are very fast [29]. This makes the void contents significantly impactful in the mechanical performance of PEEK 3D prints as crack initiation in these defects can lead to brittle failure. For this reason, PEEK samples with higher porosity percentages or lower density display lower strength [21,26]. As these voids are created in the interfaces between the elliptical cross-sections of the deposited material, their size and geometry can vary depending on the line dimensions and orientation. For, instance, layer height can be related to the number of interfaces for layer detachment and consequently to the number of voids in a 3D printed sample. PEEK samples printed with layer heights of 0.3 mm to 0.35 mm have resulted in higher tensile strength [26]. Still, excessive layer height can also result in less contact between adjacent lines and produce larger scale void defects. Perhaps for this reason, the results for strength from Design of Experiment (DoE) studies seem to favour thinner layers [30–33].

Still, aside from the effects of the mentioned parameters in the void contents of PEEK 3D prints, the research on the influence of other parameters seems scarce. Studies in the FFF with other materials have reported that a negative line-to-line distance (overlapping lines) and interlayer line translation can be used to reduce the void contents of a 3D print [34,35]. However, to the authors' knowledge, only the negative line distance was tested for PEEK with promising results since the samples increased in strength and modulus [36]. This suggests that further improvements in the mechanical properties of PEEK 3D prints can be achieved through different approaches to reduce the void contents of PEEK samples and obtain denser prints.

In this paper, the tensile and flexural properties of 3D printed PEEK are improved through FFF parametrization with the goal of documenting novel approaches to process optimization for different load configurations. This work is focused on 3D printing parameters which can influence the interfacial adhesion and the void contents of PEEK samples such as printing temperatures, line height and filament material flow. For this, Design of Experiment studies using the Taguchi approach and Analysis of Variances (ANOVA) are conducted to determine the best parameter combinations for both tensile and flexural properties. Following these results, different approaches are tested to further improve the mechanical properties of PEEK prints such as the reduction of void contents through interlayer line translation and the increase of crystallinity and interfacial adhesion through high temperature annealing treatments. With these approaches, it was possible to obtain significant increases in both the tensile and flexural properties of PEEK 3D prints.

2. Materials and methods

2.1. Materials and equipment

Industrial grade neat PEEK filament (Apium PEEK 450 Natural,

Apium Additive Technologies GmbH, Karlsruhe, Germany) with a diameter of 1.75 mm was used to print the samples. The filament was previously dried in the Apium F300 filament dryer for 4 h at 120 °C and then maintained at 60 °C for conditioning and printing. The datasheet for this PEEK grade informs that it has a glass transition and melting temperatures of 143 °C and 342 °C respectively, an elastic modulus of 4 GPa and tensile strength of 98 MPa [37].

The samples were printed using an Apium P220 printer (Apium Additive Technologies GmbH, Karlsruhe, Germany) which is designed for high-temperature printing. This printer includes an extruder liquid-cooling system which has been shown to improve filament feeding and improve flow stability [38]. Additionally, the APIUM P220 also includes an adaptive heating system around the nozzle, henceforth referred to as zone heater, which consists of a resistance heating surface placed around the nozzle that improves layer adhesion and dimensional accuracy by heating and controlling cooldown rates of the uppermost layers. A similar approach to deposition zone preheating was implemented by Hu et al. [39] where a heat collector around the nozzle helped increase the crystallinity and improve the mechanical properties of 3D printed PEEK. With these materials and equipment, high-quality samples were obtained using different printing parameters.

2.2. Design of experiments

For the Design of Experiments (DoE), the Taguchi method was used to investigate the optimal printing conditions using a reduced set of experiments. In this work, the L9 Taguchi orthogonal array was used to study the effects of 4 different printing parameters which were varied at 3 levels. The tested parameters were selected for their possible impact in the interfacial adhesion between layers and lines during the printing process. Concerning this, the selected parameters include the nozzle temperature (NT) as it influences the viscosity and bonding conditions, the zone heater temperature (ZHT) as it affects the deposition zone's temperature and cooldown rates, the layer height (LH) for its relation to the number of interlayer interfaces in the print and lastly, the extruder multiplier (EM) which is a factor applied to the flow of material through the nozzle and scales line dimensions.

Default printing settings previously used for good-quality PEEK prints were used as the level 2 of the Taguchi Design and the tested parameters were varied around these values to assess the effects of increases and decreases of the default printing parameters. With this, Table 1 displays the 9 combinations of printing parameters corresponding to the L9 array. For repetition, three samples of each combination were submitted to each mechanical test and the results were used in the Analysis of Variances (ANOVA) to determine the optimal parameter values and respective contributions. The analysis of the results was performed using the Minitab statistical analysis software (version 19.2020.1).

2.3. PEEK samples' 3D printing and testing

The slicer software Simplify3D (v4.1.2) was used to generate the G-code printing files for each of the parameter combinations. Apart from the varied parameters, all the samples were printed using a nozzle of 0.4 mm of diameter and with 100 % infill of the concentric pattern. The concentric pattern was chosen to avoid line discontinuity in the transition between the narrow and broad sections of the tensile specimens. To use the concentric pattern, all layers were considered as top/bottom layers and the wall line count was set to 2 with an outline overlap percentage of 75 %. The build plate temperature was kept at 130 °C and the printing speeds were set to 2000 mm/min for printing movements, 4800 mm/min for travel movements and 800 mm/min for the first layer printing (40 % underspeed). Additionally, all samples had to be printed with a large brim to avoid detachment from the build plate and to minimize warping issues. The brim line count was set to 30 which results in a brim width of about 12 mm.

Table 1
Taguchi Array L9 with the chosen 4 printing parameters varied in 3 levels.

	NT (°C)	ZHT (°C)	LH (mm)	EM
C1	475	110	0.1	0.9
C2	475	130	0.2	1
C3	475	150	0.3	1.1
C4	485	110	0.2	1.1
C5	485	130	0.3	0.9
C6	485	150	0.1	1
C7	495	110	0.3	1
C8	495	130	0.1	1.1
C9	495	150	0.2	0.9

With these parameters, a set of three tensile test specimens and three flexural test specimens were printed for each of the L9 array combinations. The tensile properties were determined following ISO 527 specifications and the printed specimens were dimensioned for type 1BA with 95 mm of overall length and 4 mm of thickness. Tensile testing was performed in universal testing machine (MTS 312.31, MTS Systems Corp., Minnesota, USA) with a 100KN load cell and constant crosshead of 0.01 mm/s to comply with the specification for an average elastic strain rate of 1 % per minute. In these tests, strain at yield was measured using an extensometer and the nominal strain was determined following method B specified in ISO 527. The flexural properties were determined according to ISO 178 guidelines and the specimens were dimensioned with the preferred dimensions of 80 mm for length and 10 mm for width. The thickness of the flexural specimens was reduced to 3 mm to comply with the test machine's capability. Flexural three-point bending tests were performed with an in-house developed flexural testing machine and at a crosshead speed of 2 mm/min.

2.4. Calorimetry

Differential Scanning Calorimetry (DSC) tests were carried out to determine the Apium PEEK 450 thermal properties and crystallinity. Testing was performed using a NETZSCH DSC 204 F1 Phoenix calorimeter (Erich NETZSCH GmbH & Co. Holding KG, Selb, Germany) and the thermal analysis was performed using the NETZSCH Proteus software. DSC testing was conducted for filament and printed filament samples at heating/cooling rate of 10 °C/min and with maximum temperature of 490 °C for 5 min. The glass transition (T_g) and melt temperatures (T_m) were obtained from the heating curve while the “hot” crystallization temperature (T_{hc}) was obtained from the cooling curve.

To determine the samples' crystallinity, the ratio between the heat required to melt the sample and the theoretical heat of fusion of fully crystalline PEEK was calculated following the same method used in other works [40–42]. With this, the percentage of the crystalline phase was determined by the equation:

$$X_c(\%) = \frac{\Delta H_{endo} - \Delta H_{exo}}{\Delta H_c} \quad (1)$$

where ΔH_{endo} is the melt enthalpy measured as the area under the melting endothermic peaks, ΔH_{exo} is the “cold” crystallization enthalpy measured as the area above the exothermic peaks of the heating curve and ΔH_c is the theoretical melt enthalpy of fully crystalline PEEK. Following the crystallinity percentage determination methods used by other authors, this theoretical melt enthalpy of fully crystalline PEEK corresponds to 130 $J.\ g^{-1}$ [43].

2.5. Porosity characterization and improvement

The porosity features of the printed specimens were firstly observed through macrographs of a cross-section of the broad section of the tensile test specimens. A sample was taken for each of the parameter combinations from the DoE study, placed in resin and polished carefully

to remove the plastic deformation region from the cut of the cross-section.

Following this, the optimal parameter combinations for both tensile and flexural strength were used to print specimens where the deposition path of the filament could decrease the porosity percentage. For this, 4 new sets of specimens were produced which included the same concentric pattern used in the DoE specimens (C10), a crossing infill pattern with alternating raster angles of 45° and −45° (C11), a concentric infill pattern with an interlayer translation of half the line width (C12) and a similar interlayer translation pattern with an alternating layer with 0.1 mm of height. The cross-section of these patterns is illustrated in Fig. 12 along with the corresponding macrographs.

For these configurations, sets of three specimens were printed using the parameters from the results of the DoE study and submitted to tensile and flexural testing. In addition to this, smaller samples were printed and submitted to X-ray microtomography (micro-CT) to analyse the 3D morphology of the void contents for different printing parameters and infill patterns. The micro-CT internal porosity analysis was performed at Micronsense-Metrologia Industrial (Leiria, Portugal) using a Phoenix V|TOME|X m 240 where the PEEK samples were scanned at 140 kV and 150 μA. The angular increment for the scanning was 0.15°, the spatial resolution 41 μm and the image data was analysed using a 3D tomographic reconstruction and analysis software (Volume Graphics 3.5.2 software, Volume Graphics).

2.6. Heat treatment

A high temperature annealing treatment was performed on a set of tensile and flexural test specimens. The annealing temperature and the heating and cooling rates were chosen according to previous works which reported increases in the crystallinity and the mechanical properties of the samples [14,41,44]. For this, the samples were placed in the centre of the furnace above a refractory plate to minimize the differences in the heat distribution between the samples. The annealing treatment was then programmed to heat at 5 °C/min up to 300 °C where the samples were kept for 4 h. After this time, the furnace door was opened and the controller was programmed to cool until the ambient temperature also at 5 °C/min. Without controlled cooling systems, the temperature measurements revealed that the samples cooled non-linearly at rates between 9 and 2 °C/min.

3. Results and discussion

3.1. Thermal properties and crystallinity

DSC analysis was performed for three filament samples taken from the spool and three samples taken after printer extrusion. Before taking the samples, the filament spool was dried in an oven heated to 120 °C for 4 h and then maintained at 60 °C to evaporate any absorbed humidity. The DSC heating and cooling curves were analysed and the results for the transition temperatures and crystallinity percentage of the filament (PEEK F) and the extruded filament (PEEK P) can be seen in Table 2.

The melt temperature obtained from the heating curve and the “hot” crystallization temperature obtained from the cooling curve, as shown in the DSC curve for the printed PEEK sample displayed in Fig. 1, were similar for filament and printed samples. However, the glass transition temperature was about 10° higher for the filament samples. None of the DSC heating curves displayed the “cold” crystallization exothermic peak as shown in other works [40,42,45] which suggests that the samples

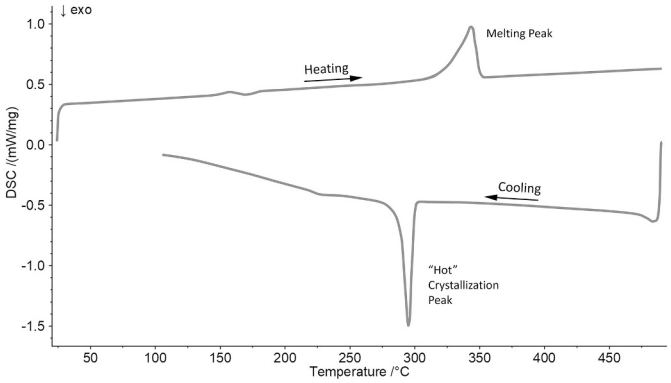

Fig. 1. Heating and cooling DSC plot for the printed PEEK sample (PEEK P).

were highly crystalline since no more crystalline phase was observed to form upon heating. The results for the samples crystalline percentage seem to confirm this as the average crystallinity percentage of 32.7 ± 2.0 % for the PEEK F samples and 33.4 ± 2.4 % for the PEEK P samples are similar to the crystallinities of non-annealed samples reported in other works [41,46] and higher than the crystallinities reported for samples which displayed “cold” crystallization peaks [42,45]. Interestingly, the PEEK F samples also displayed a secondary melting endothermic peak (T_{m2}) typically observed in annealed samples. This secondary melt temperature of 223.6 °C is typical of low temperature annealing treatments as reported by Regis et al. [41]. This is likely attributed to the filaments manufacturing process since the filament drying is performed below the glass transition. Furthermore, the printed filament samples were taken right after extrusion which means the corresponding cooldown rates should be higher than the cooldown rates of printed lines in an actual print. This suggests that the thermal processing involved in the samples 3D printing does not significantly affect the samples crystallinity.

3.2. Mechanical properties

3.2.1. Tensile properties

The results for strength and modulus from the tensile tests can be seen in Fig. 2. The highest tensile strength of 86.7 MPa together with the second highest tensile modulus of 3.36 GPa were obtained with the parameter combination C8 which corresponds to a nozzle temperature of 495 °C, zone heater temperature of 130 °C, 0.1 mm of layer height and an extruder multiplier of 1.1. The second highest tensile strength of 83.8 MPa along with the highest tensile modulus of 3.71 GPa were displayed by C6 which was printed with the nozzle at 485 °C, the zone heater at 150 °C, a layer height of 0.1 mm and an extruder multiplier of 1. Although no clear tendency can be observed with any of the tested parameters, the results for strength and stiffness seem to be associated with the void area observed in the samples' macrographs (Fig. 3). The cross-sections of the samples C8 and C6 show little presence of smaller scale void defects and correspond to the denser prints whereas samples C1 and C3, which correspond to the lowest observed tensile strength and modulus, display more voids of larger scale.

The void contents of sample C1 can be attributed to the under extrusion since the lowest value for the extruder multiplier produces thinner lines and results in poor interline adhesion. Conversely, sample C6 combines the highest layer height with the highest extruder

Table 2
DSC results for thermal properties and crystallinity percentage.

	T_g (°C)	T_{m2}(°C)	ΔH_{m2} (J. g^{-1})	T_m (°C)	ΔH_m (J. g^{-1})	T_{hc} (°C)	ΔH_{hc}	X_c (%)
PEEK F	165.2 ± 2.3	223.6 ± 0.7	2.08 ± 0.13	341.8 ± 0.1	40.45 ± 2.43	284.0 ± 0.3	−40.02 ± 0.47	32.7 ± 2.0
PEEK P	154.8 ± 6.1	–	–	341.7 ± 1.1	43.40 ± 3.12	282.8 ± 12.2	−40.80 ± 5.84	33.4 ± 2.4

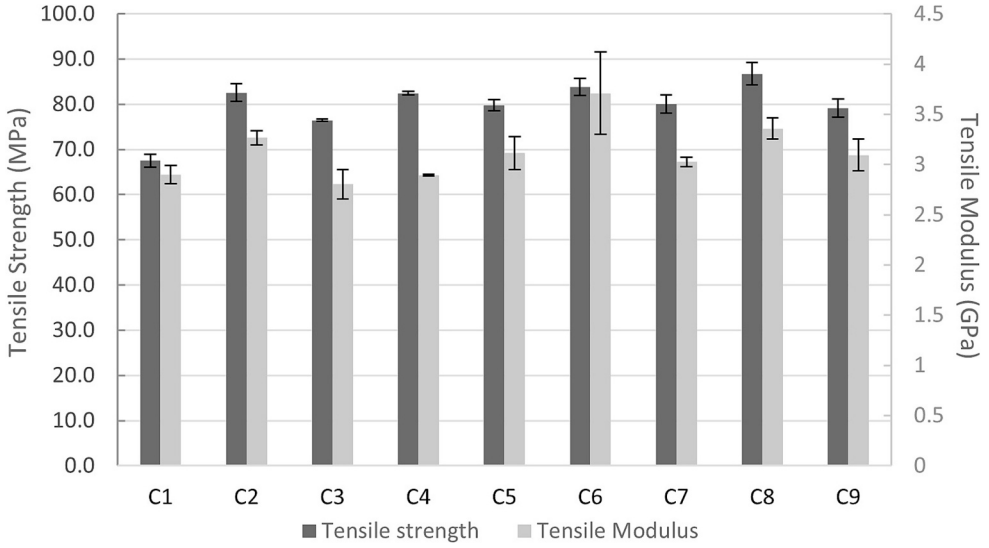

Fig. 2. Tensile properties for the L9 Taguchi array parameter combinations.

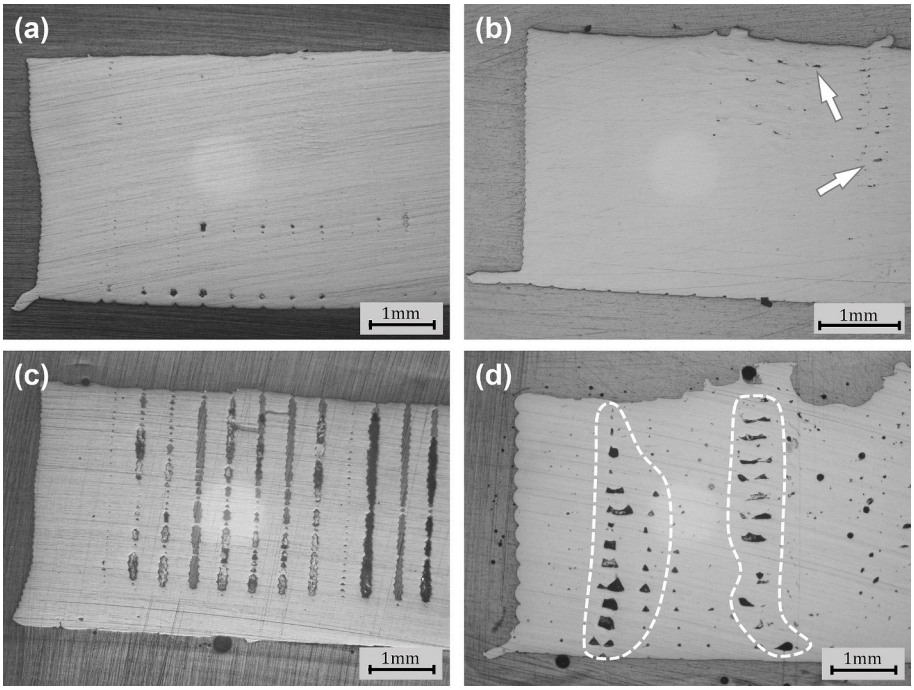

Fig. 3. Macrographs of cross-sections of the tensile specimens C6 (a), C8 (b), C1 (c) and C3 (d). White arrows and contouring mark the void defects caused by over extrusion.

multiplier which results in a significant over extrusion. This seems to create instability issues with the material flow through the nozzle where the excessive flow builds pressure in the nozzle and disturbs the extrusion flow. These instabilities in the extrusion flow result in the void defects marked by the white arrows and contouring in Fig. 3 which can vary in scale depending on the amount of over extrusion. These defects can be the reason why over extruded samples such as C3 and C4, despite appearing denser, show worse results in the tensile tests.

These issues with over extrusion are also shown in the results for the signal-to-noise (SN) ratio's main effects from the Taguchi analysis which can be seen in Figs. 4 and 5. Although the increase of the extruder multiplier can produce denser prints, the optimal parameter combinations for both tensile strength and tensile modulus favours the default value of 1 for the EM. Similarly, the optimal parameters also include default values of 485 °C for NT and 130 °C for ZHT concerning both the tensile strength and tensile modulus. For the layer height, however, the results differ where the minimum LH of 0.1 mm is preferred for the samples rigidity while the results for tensile strength favour the default LH of 0.2 mm.

Despite the similar optimal parameters, the results from the ANOVA for the tensile modulus (Table 3) and for the tensile strength (Table 4) are in less agreement. For the samples' strength, the highest contributions of about 30 % are attributed to the EM and NT parameters while LH displayed the lowest contribution of just 4.2 %. For tensile strength all parameters showed statistical significance, however this is not the case for the samples' rigidity. Concerning the tensile modulus, NT was just below statistical significance with a *p*-value of 0.063. For this reason NT was pooled which resulted in an increase the contribution of the error. In

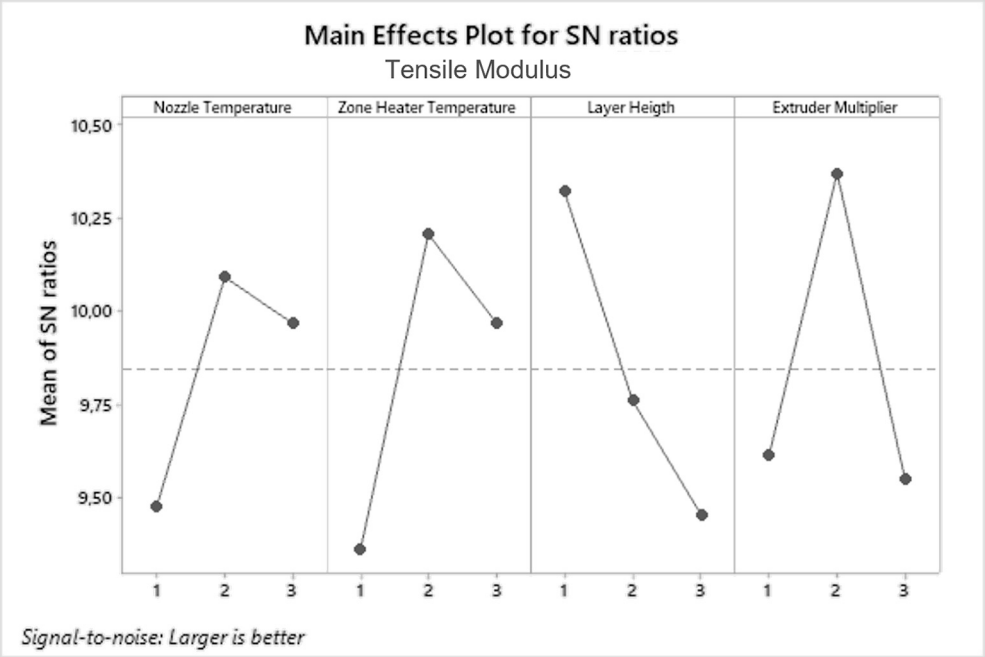

Fig. 4. Tensile modulus main effects plot for SN ratios.

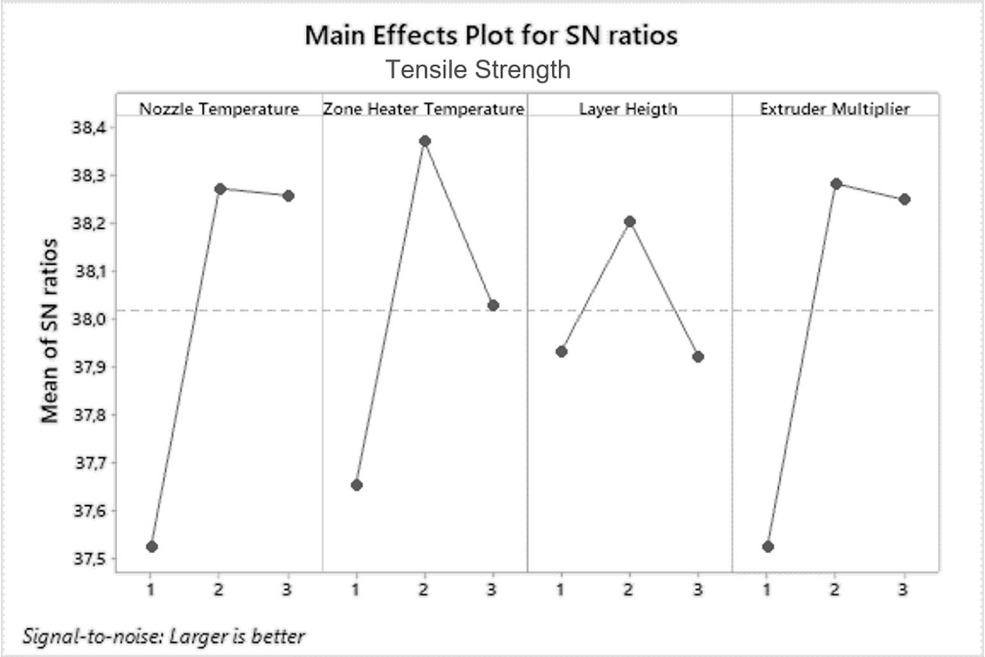

Fig. 5. Tensile strength main effects plot for SN ratios.

Table 3
ANOVA results for tensile modulus.

	Degrees freedom	Sum of squares	Mean square	F-value	P-value	Contribution (%)
NT	Pooled					
ZHT	2	0.4930	0.2465	4.51	0.024	18.3
LH	2	0.5522	0.2761	5.05	0.017	20.4
EM	2	0.5657	0.2829	5.18	0.015	20.9
Error	20	1.0931	0.05466			40.4
Total	26	2.7041				

Table 4
ANOVA results for tensile strength.

	Degrees freedom	Sum of squares	Mean square	F-value	P-value	Contribution (%)
NT	2	252.75	126.377	29.32	0.000	31.4
ZHT	2	181.66	90.830	21.07	0.000	22.6
LH	2	34.08	17.042	3.95	0.038	4.2
EM	2	257.57	128.787	29.88	0.000	32.1
Error	18	77.59	4.310			9.7
Total	26	803.66				

any case, ZHT, LH and EM all presented similar contributions between 18 and 21 % which suggests that the selected parameters, apart from NT, all have similar impact in the samples' tensile modulus.

In the results for both strength and modulus, the extruder multiplier parameter displays heavier contributions as this parameter is directly related to the amount of material used in the print and therefore, is related to the samples density. Denser PEEK prints correspond to larger effective cross-section areas for load support and result in higher strength and modulus [21,26]. However, the differences in the contributions of the other parameters for strength and modulus can be more difficult to assess. The tensile loading of the printed samples can be supported differently depending on the samples macrostructure as shown in the macrographs (Fig. 3). Considering the tensile strength, the maximum load supported could be related to the interfacial adhesion of the print. If the printed lines yield separately, the cross section area under elastic deformation starts decreasing which should lower the maximum load supported. This could be the reason why the effect of the nozzle temperature is more significant for the tensile strength since the molecular bonding of the printed lines could prevent them from yielding separately. This can be seen in the fracture surface of sample C1 (Fig. 6) where the stronger adhesion regions marked by the blue contour yielded and fractured separately of the poor adhesion region contoured in yellow which yield and fracture in groups of vertically bonded lines as seen in Fig. 3c.

For the samples' stiffness however, the effective cross-section area could be a more important factor at play thus favouring larger lines and denser prints. This could explain the contribution of layer height in the results for tensile modulus. In any case, calibration of the extrusion flow could be the most effective way of increasing the density of PEEK prints and, by consequence increase their tensile strength and stiffness. For this, the required amount of extrusion to produce dense prints without injuring flow stability needs to be calibrated according to the other parameters used and the deposition path of the 3D print.

3.2.2. *Flexural properties*

The results for the flexural strength and modulus from the three-point bending tests are displayed in Fig. 7. In this case, the tensile strength and the tensile modulus seem to vary together which could mean that the tested parameters have similar effects in both the samples' strength and stiffness. The highest values of 128.3 MPa for flexural strength and 3.11 GPa for the flexural modulus were obtained with the parameter combination C3 corresponding to a NT of 475 °C, ZHT of 150 °C, LH of 0.3 mm and EM of 1.1. The second and third highest values for both the flexural strength and modulus were obtained for combinations C8 and C4 respectively. Here, a clear trend can be observed where the combinations C3, C8 and C4 were the only three combinations from the Taguchi array where the extruder multiplier value of 1.1 was used. Furthermore, the bottom three flexural strengths were obtained for combinations C1, C5 and C9 which correspond to the three samples where the minimum value for EM of 0.9 was used. The extruder multiplier's effects on the flexural properties seem to overwhelm the effects of other parameters. Similar to what was observed with the tensile specimens, the higher values of EM are related to lower void contents provided that the samples do not present excessive over extrusion where flow stability void defects are created. In the flexural specimens, the extruder multiplier of 1.1 appears more adjusted to the 3D printing of sample C3 than with the tensile specimen where the effect of over extrusion on the surface of sample C3 is highlighted by the yellow contour (Fig. 8). Once again, extrusion calibration appears to have significant effects on the mechanical performance of a 3D printed component.

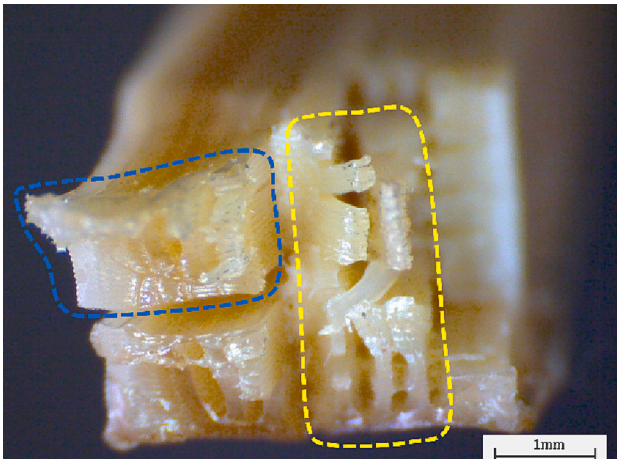

Fig. 6. Fracture surface morphology of C1. Weaker bonding region contoured in yellow and stronger bonding region contoured in blue. (For interpretation of the references to colour in this figure legend, the reader is referred to the web version of this article.)

The effects of other parameters are more difficult to observe. The loads on the 3D printed specimen created by the flexural testing create shear in the interfaces between layers and, for this reason, layer adhesion could be especially important for the samples' flexural properties. This can be the reason why samples C3 and C8, which were printed with higher temperatures either for the nozzle or for the zone heater, performed better than C4. Higher printing temperatures have been related to improvements in the interlayer adhesion of PEEK prints [16]. Additionally, larger layer height also reduces the number of layer interfaces which are subject to shear stresses. Interlayer bonding interfaces are usually the weakest part of the print since the temperature difference between lines of consecutive layers is larger than the difference between consecutive printed lines, even if the relative position between the lines is equivalent [47]. This means that reducing the number of these weak interfaces subject to shear stresses using larger layer heights could improve the flexural properties of 3D printed parts. However, no significant differences were observed in the two highest flexural strengths and stiffnesses for samples C4 and C8 which were printed with LH of 0.3 and 0.1 mm respectively.

The Taguchi analysis results for the flexural properties of the printed PEEK specimens differ from the results for the tensile properties. The main effects' plots for SN ratios of both the flexural modulus (Fig. 9) and the flexural strength (Fig. 10) present the same optimal parameter combination. The Taguchi analysis results show that optimal parameter combinations for both flexural strength and modulus corresponds to the maximum values for all the tested parameters which consists of a NT of 495 °C, ZHT of 150 °C, LH of 0.3 mm and an EM of 1.1. This can be explained by the expected effects for each of the tested parameters in the interlayer adhesion of PEEK 3D prints which seem more significant in the support of the shear and tensile/compressive loads above and below the neutral plane during the samples bending.

In addition to this, ANOVA results as seen in Tables 5 and 6 show that the extruder multiplier displays the highest contribution for both strength and modulus, especially concerning the flexural strength where EM was statistically significant and attributed a contribution of 85.6 %. However, the statistical significance of the selected parameters is questioned by the ANOVA results since all factors displayed considerably high *p*-values in the analysis for the flexural modulus. Regarding flexural strength, both ZHT and LH do not display statistical significance with p-values of 0.390 and 0.063 respectively. After pooling ZHT for the flexural strength, the p-value of LH decreases suggesting an increase in its statistical significance despite still siting just outside the confidence condition of $p > 0.05$. Nevertheless, these results seem to attest to the improvement of the flexural properties of PEEK 3D prints through extrusion calibration to obtain denser samples and higher printing temperatures to increase interfacial adhesion.

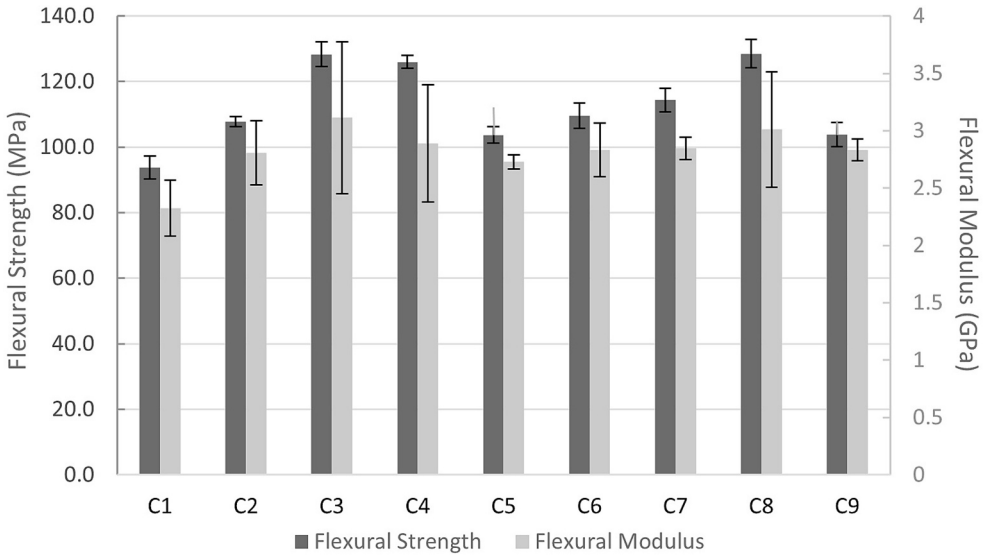

Fig. 7. Flexural properties for the L9 Taguchi array parameter combinations.

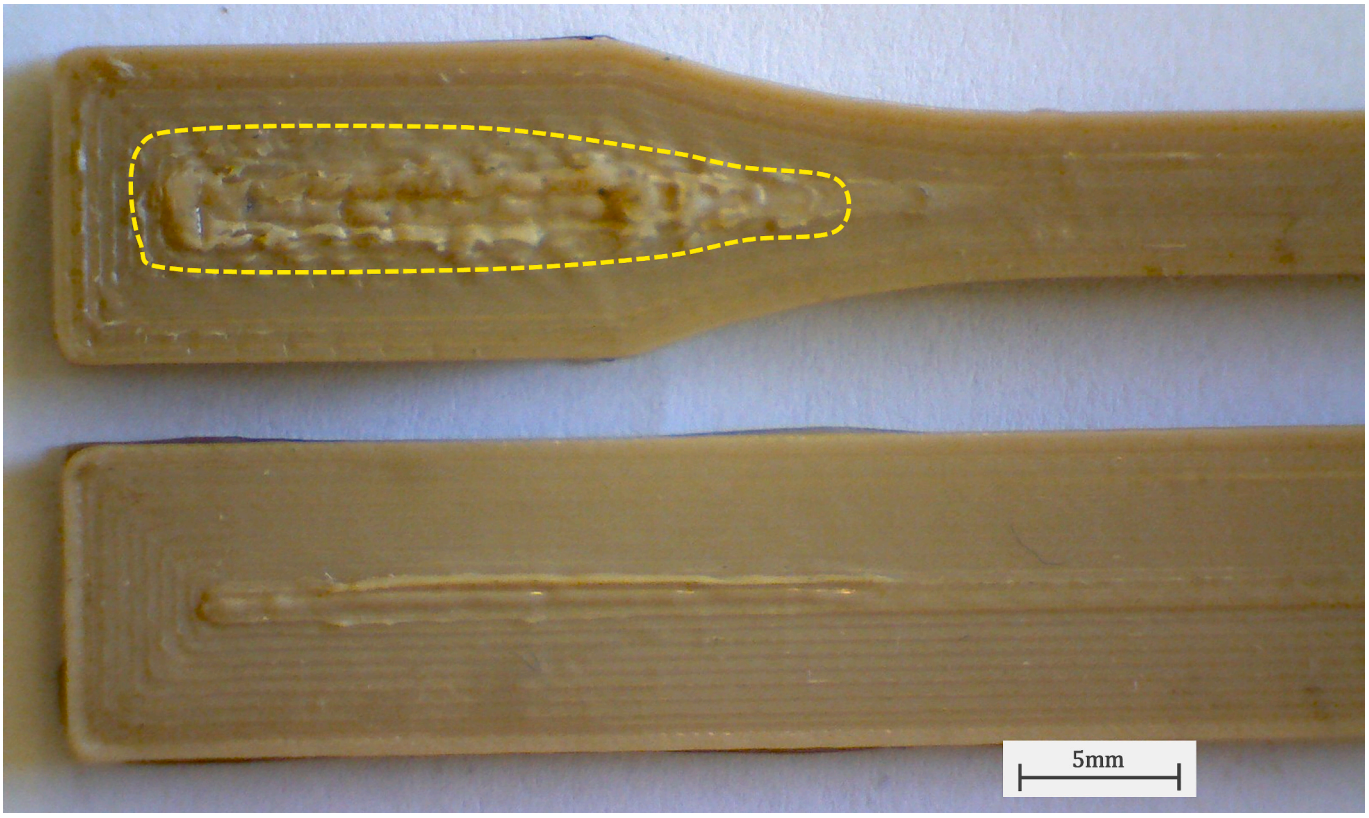

Fig. 8. Extruder multiplier of 1.1 effects on the surface quality of the tensile (a) and flexural (b) specimen C3. Yellow contouring marks the surface defects caused by the nozzle on over extruded material. (For interpretation of the references to colour in this figure legend, the reader is referred to the web version of this article.)

3.2.3. Improvement of the mechanical properties of PEEK 3D prints

With the results from the Taguchi analysis, the optimal parameter combinations for tensile and flexural strength were used to print corresponding test specimens (C10). Concerning the flexural test specimens, the extruder multiplier of 1.1 from the optimal parameter's results was producing significant over extrusion in samples C10 (Fig. 11) which was creating severe flow instabilities and resulting in poor quality prints. For this reason, all flexural test specimens in this section were printed with the default extruder multiplier of 1.

In addition to this, the g-code printing files for these combinations were modified to produce different infill configurations which could reduce the internal void percentage of the prints. For this, three different infill configurations were tested, one where the infill line angle alternates between 45° and −45° (C11), one with interlayer line translation of half the line width (C12) and another with the same line translation but also with an alternating layer height of 0.1 mm (C13). The tested infill configurations are schematically illustrated in Fig. 12 along with the macrographs of the respective printed samples' cross-sections.

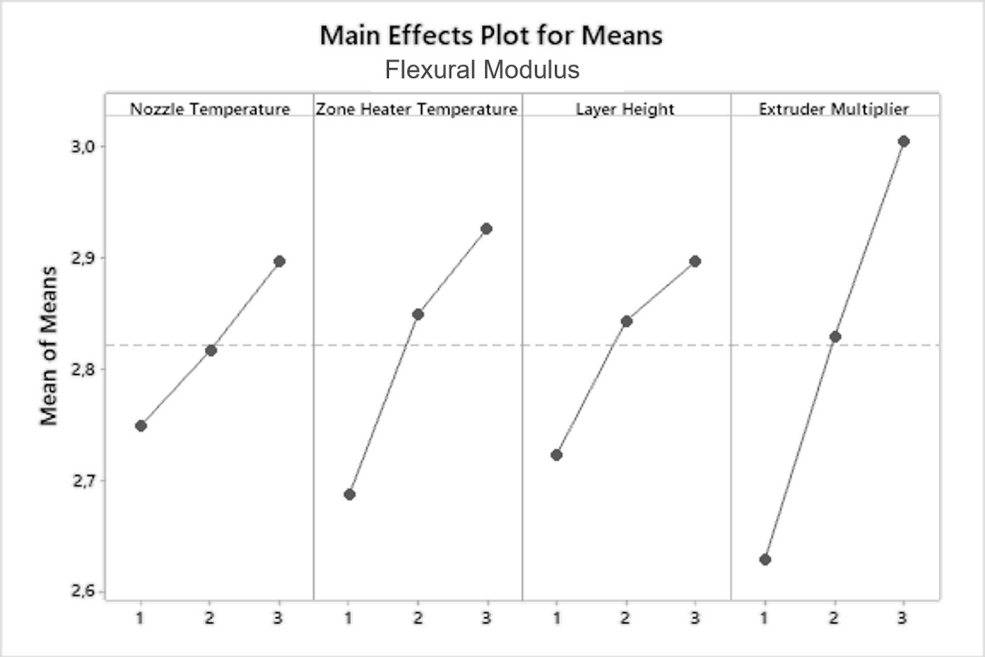

Fig. 9. Flexural modulus main effects plot for SN ratios.

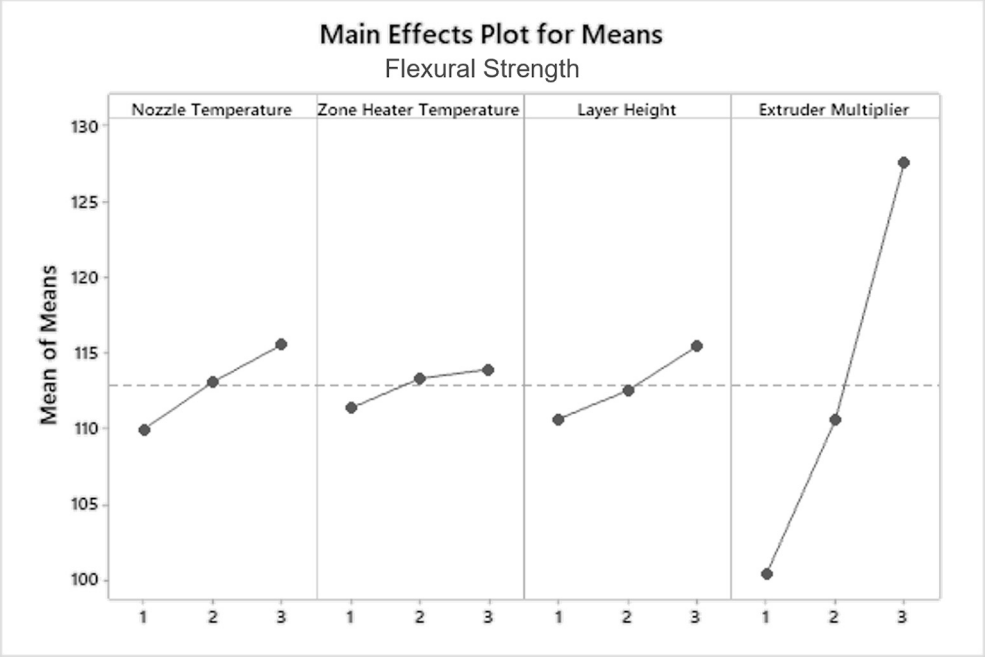

Fig. 10. Flexural Strength main effects plot for SN ratios.

Table 5
ANOVA results for flexural modulus.

	Degrees freedom	Sum of squares	Mean square	F-value	P-value	Contribution (%)
NT	2	0.09815	0.04907	0.25	0.780	2.10
ZHT	2	0.26966	0.13483	0.69	0.514	5.79
LH	2	0.14340	0.07170	0.37	0.698	3.08
EM	2	0.63541	0.31770	1.63	0.224	13.63
Error	18	3.51469	0.19526			75.40
Total	26	4.66130				

Table 6
ANOVA results for flexural strength.

	Degrees freedom	Sum of squares	Mean square	F-value	P-value	Contribution (%)
NT	2	140.47	70.23	4.31	0.027	3.54
ZHT	Pooled					
LH	2	106.13	53.06	3.26	0.059	2.68
EM	2	3392.97	1696.49	104.21	0.000	85.57
Error	20	325.58	16.28			8.21
Total	26	3965.15				

Fig. 11. Surface quality of flexural test specimen C10 printed with an extruder multiplier of 1.1.

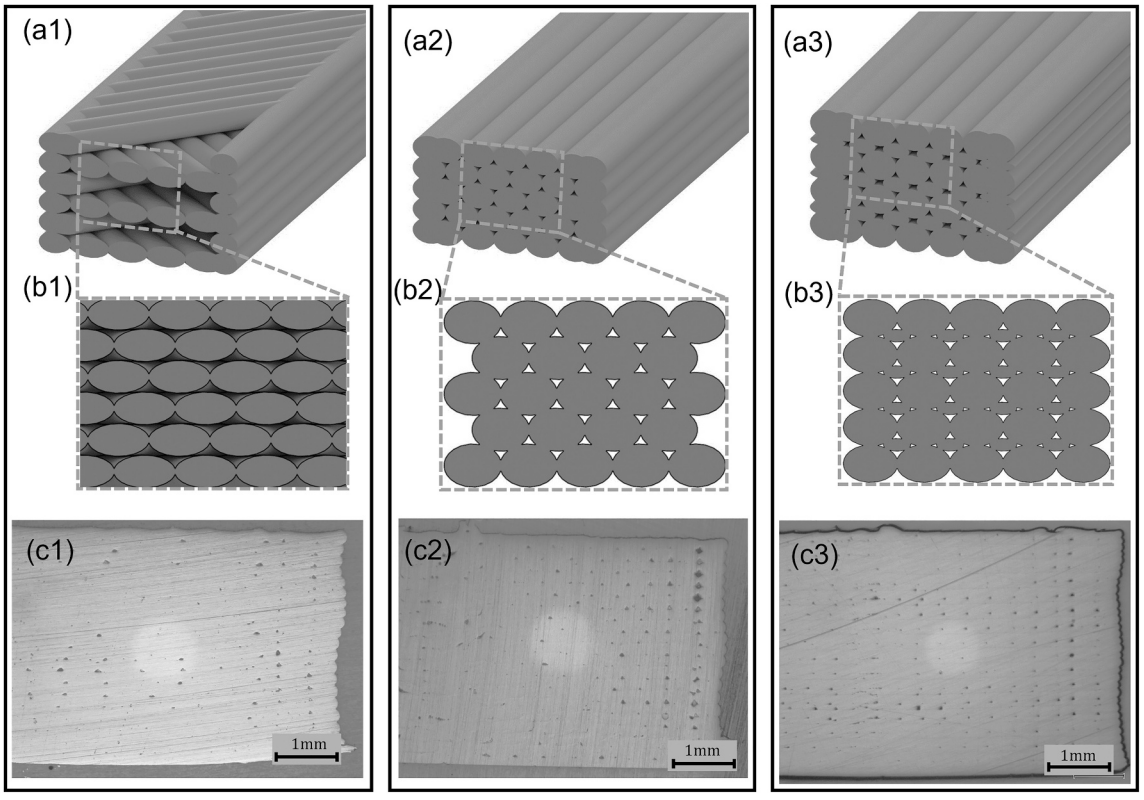

Fig. 12. Schematic representation of the infill configuration's macrostructure for samples C11 (a1), C12 (a2) and C13 (a3) and the corresponding cross-section illustration (b1, b2, b3) and micrograph (c1, c2, c3).

The macrographs of the cross-sections of the tested infill configurations (Fig. 12c) suggest that the samples display a low void volume percentage resembling the cross-section of sample C8 (Fig. 3) which resulted in the highest tensile and flexural strengths from the Taguchi experiments. Although the presence of void defects between the printed lines can still be observed, the average void size seems smaller for the tested infill configurations. Furthermore, each configuration results in different void morphology and placement that could have different effects in the printed samples' load support.

The alternating infill line angles of sample C11 increases the number of lines in contact from consecutive layers and makes them more interconnected. With this configuration, the voids between lines of the same layer are also placed in an alternating angle configuration which seems to make the voids more irregular and smaller in scale compared to the voids created with the other configurations which are more longitudinally uniform. For the case of the interlayer translation configurations C12 and C13, the line offset also doubles the number of lines in contact between layers. This approach to deposition has been previously studied for 3D printed ABS and resulted in a reduction of the void size and volume of the samples [35]. Additionally, the offset places the lines above the longitudinal notch created between the elliptical cross-sections of the printed beads which could also reduce the void size and volume. Moreover, the configuration used for C13 used smaller scale lines to fill this gap where the void size could be reduced further. For these reasons the infill configurations used in samples C11, C12 and C13 have the potential to lower void volume and improve interactions

between layers.

Although the effects of these infill configurations in the void contents of PEEK prints can be investigated geometrically, the accuracy of this analysis can be questioned given the complexity of the interactions present in FFF deposition. The macrographs of the 3D printed samples' macrostructure correspond to a specific cross-section, and therefore correspond to a very limited representation of the void contents even for the longitudinal infill configurations. Considering this, smaller scale 25 × 20 × 5 mm samples of configurations C10, C11, C12 and C13 were submitted to micro-CT porosity analysis along with samples printed with the parameter combinations C1 and C6 which represent low and high strength samples from the DoE study, respectively. The 3D overview of void defects highlighted by volume (Fig. 13) provides a clear view of the tested samples void volume and morphology. In addition to this, the porosity analysis results for the number of voids, void volume and porosity percentage are included in Table 7.

As expected, sample C1 displays the largest overall volume of voids which are also significantly larger in size. The reason for this high void volume percentage, as already mentioned, is attributed to the lower printing temperatures and EM of 0.9 which produce overly thin lines and results in poor interline adhesion as seen in Fig. 3c. In turn, sample C6 displays significantly lower void volume compared to sample C1 where the larger size voids seem to be mostly present in the top layers. Void size increases with layer count since the bottom layer are compacted against the build plate which makes the surface of contact between lines greater for the bottom layers [48]. Sample C10 which was printed with the

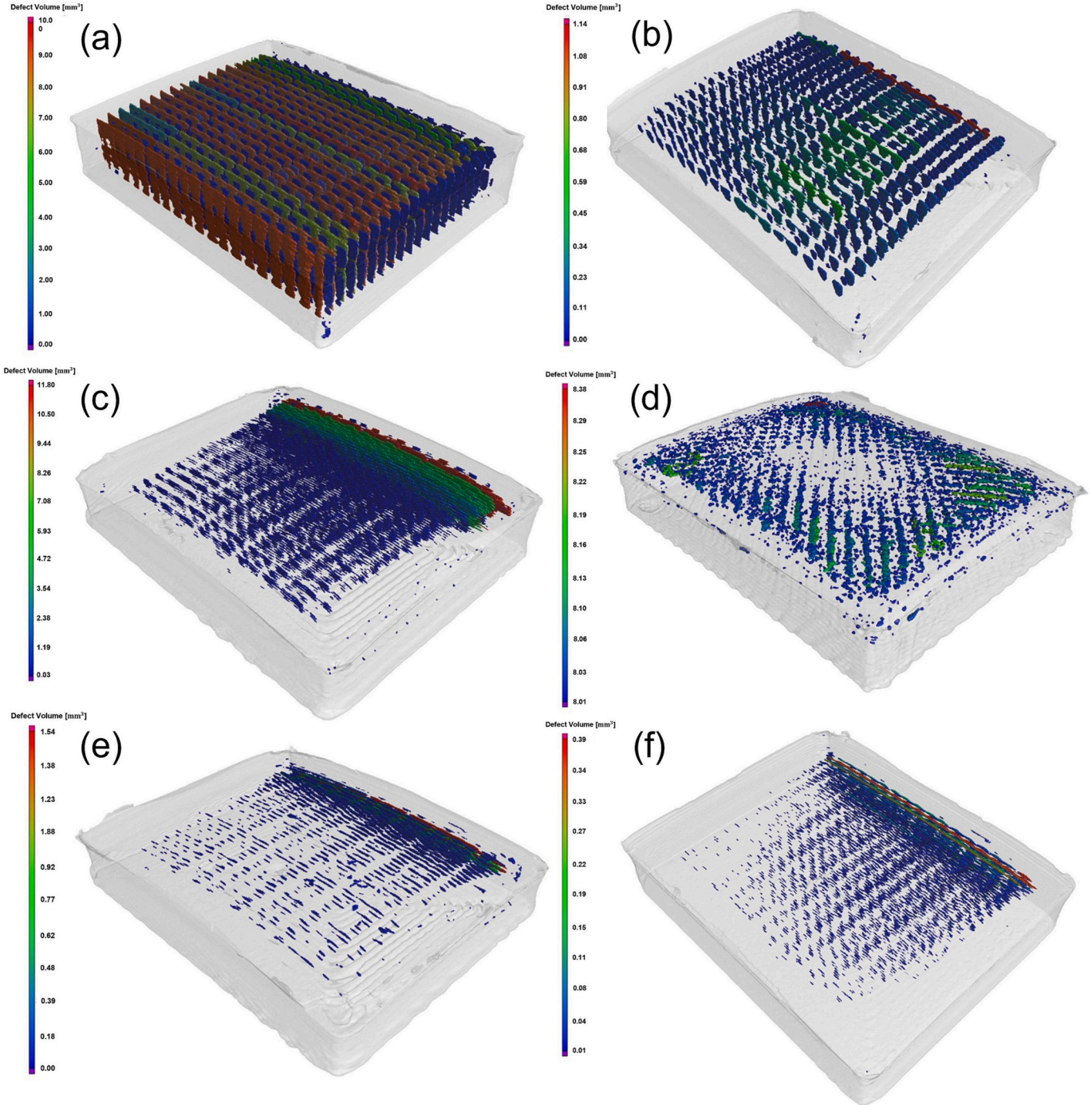

Fig. 13. Micro-CT porosity analysis of void defect volume 3D overview for samples C1 (a), C6 (b), C10 (c), C11 (d), C12 (e) and C13 (f).

Table 7
Micro-CT porosity analysis results.

	Number of voids	Number of voids bigger than		Void volume (mm^3)	Void percentage
		0.15 mm^3	0.1 mm^3		
C1	1061	–	–	224.25	9.81 %
C6	697	40	–	31.91	1.38 %
C10	2372	23	–	49.45	2.12 %
C11	3439	–	20	24.37	1.05 %
C12	1199	–	1	11.29	0.51 %
C13	3377	–	7	13.19	0.56 %

optimal parameter combination for tensile strength was revealed to contain a larger void volume and count than sample C6. However, a concentration of larger scale voids can be observed near one of the top longitudinal edges of the C10 print, which can be attributed to warping defects. Despite the higher void volume, the number of voids bigger than 0.15 mm^3 is lower in C10 which means that sample C10 displays smaller scale void defects than sample C6.

Apart from this, micro-CT porosity analysis results (Table 7) show that the tested infill configurations represented in Fig. 12 were successful in decreasing the void volume of the PEEK prints. Compared to C6, which can be considered a low porosity PEEK print, the infill configurations C11, C12 and C13 were able to reduce the void volume by 24–65 %. Of these samples, the lowest void size and volume was achieved by the interline translation configuration C12 closely followed by C13. Despite the use of smaller beads to fill the notch between the printed lines, configuration C13 produced more voids bigger than 0.1 mm^3 compared to C12. As these results show, it is possible to significantly decrease the void contents of 100 % infill PEEK prints through designed infill line placement and without the increase of extrusion flow. Since denser PEEK prints have been associated with higher strength [21,26], these configurations are expected to increase the mechanical properties of samples printed with given parameters.

Tensile and flexural test specimens for configurations C10, C11, C12 and C13 were printed and tested to relate the decreases in void contents of the different infills to the samples' mechanical properties. The results for the tensile and flexural properties are shown in Figs. 14 and 15 respectively which also include the properties of the highest strength sample obtained in the Taguchi studies for comparison. Given the issues of over extrusion mentioned above for the flexural specimens (Fig. 11), the highest strength sample printed with an EM of 1 was chosen from the Taguchi array for comparison which corresponds to combination C7. Concerning these issues, two over extruded samples corresponding to C13 printed with an EM of 1.1 and C10 printed with EM of 1.05 were still submitted to flexural testing despite their defective surface quality and yielded interesting results. The over extruded C10 specimen resulted in a flexural strength of 146.7 MPa and a flexural modulus of 3.44 GPa while C13 resulted in a flexural strength of 148.6 MPa and a flexural modulus of 2.39 GPa. These results can suggest that high strength samples can be produced through excessive over extrusion. However, the excessive material flow was immersing the nozzle mid print which could damage both the extruder and the zone heater. For this reason, the use of the EM of 1.1 was discarded despite the significantly higher results for flexural strength.

The results for the tensile and flexural properties of sample C10 closely match the strength and stiffness of the highest strength samples C8 and C7 from the DoE study. This gives some validity to the Taguchi analysis results since the samples C10 were printed with the optimal parameter combinations for strength. Concerning the tensile properties, the alternating angle configuration C11 displayed the highest value of both tensile strength and modulus. The alternating angle in infill seems to support tensile loading better than the line alignment with the loads. This can be explained by a "scissoring" effect where tensile load energy for deformation is spent on straightening the infill lines. A similar effect has been reported for the tensile loading of carbon fibre/epoxy composites [49]. Provided that the adhesion between lines is strong, the energy spent on this effect is added to the energy spent on the deformation of the samples and thus results in higher peak tensile loads.

Apart from this, the interlayer translation configurations C12 and C13, despite little increases in stiffness, displayed lower tensile strengths than C10 and C8. Conversely, in the flexural testing, the configurations C12 and C13 yielded the best results. This can be explained by the improvement in the interactions between lines of consecutive layers with C12 and C13 which reduce the effects of shear stresses in the interfaces between layers that were previously mentioned. With this, configuration C12 corresponding to the lowest void percentage resulted

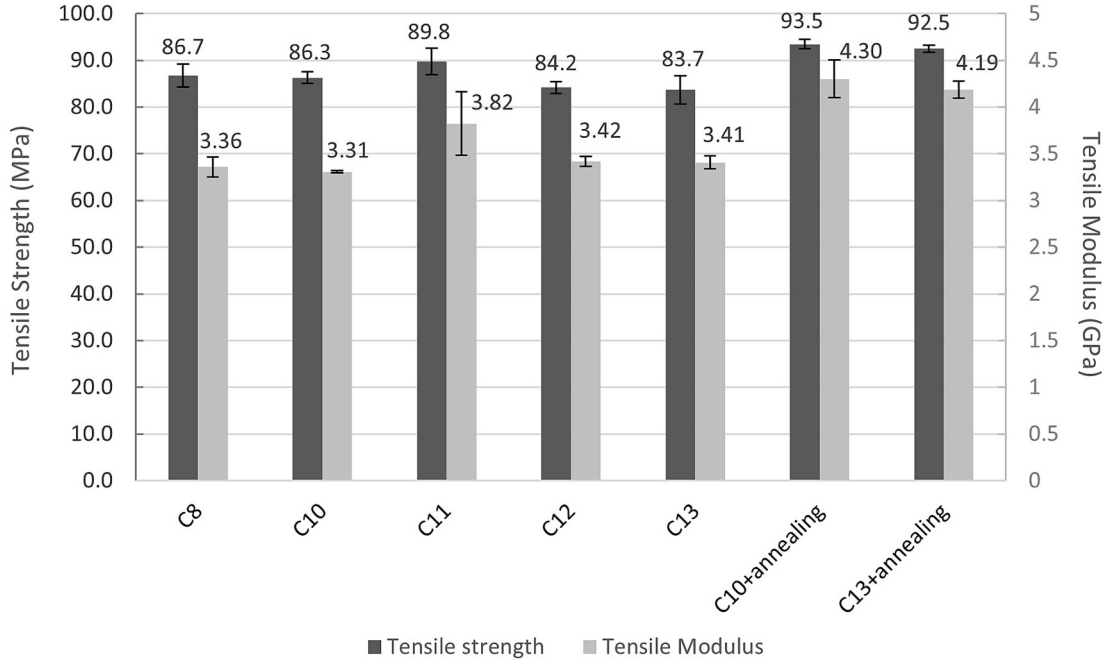

Fig. 14. Tensile properties of the samples with different infill configurations including annealed samples.

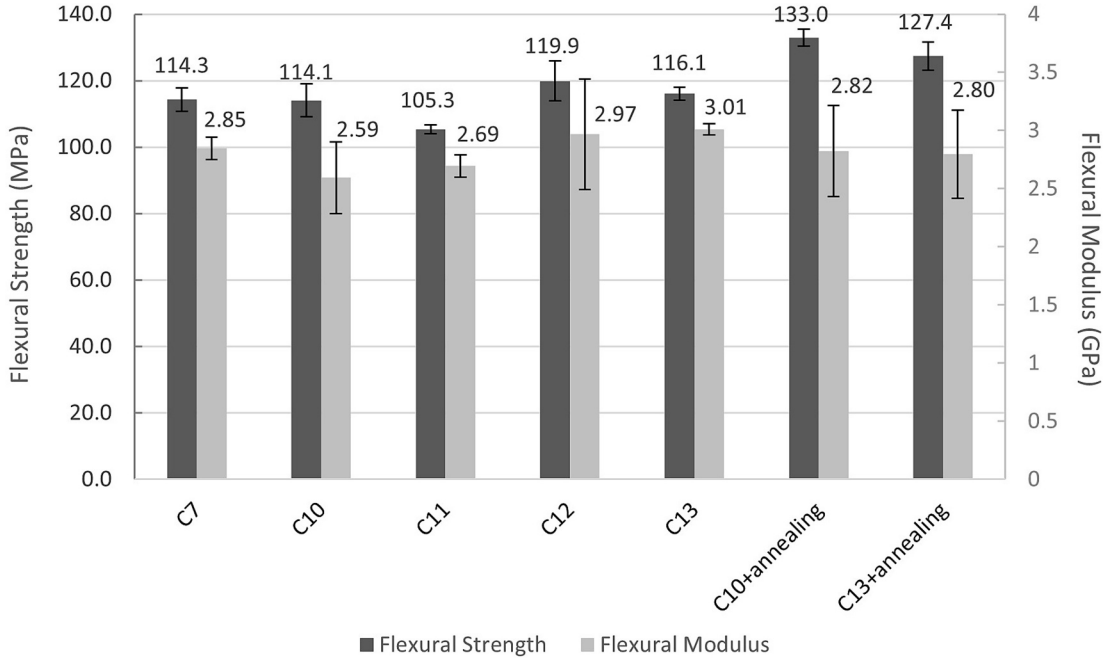

Fig. 15. Flexural properties of the samples with different infill configurations including annealed samples.

in the highest flexural strength. Compared to C10, the best performing infill configurations achieved an increase of 4.1 % in tensile strength and 15.4 % in tensile modulus for C11 and increases of 5.1 % in flexural strength and 4.2 % in flexural modulus for C12.

Lastly, high-temperature annealing treatments were performed in samples C10 and C13 to test for further increases in these samples' tensile and flexural properties. The tensile strength of the annealed samples increased the strength of C10 by 8.3 % and of C13 by 10.5 % but the highest increases were seen in the samples' modulus where C10 was increased by 29.9 % and C13 by 22.9 %. These substantial increases in stiffness can be very relevant for the use of 3D printed PEEK in orthopaedic medical applications where the stiffness of human bone is to be matched [50]. Conversely, the flexural modulus increased 8.9 % for C10 and decreased 6.7 % for C13 while the flexural strength displayed higher increases of 16.6 % for C10 and 9.7 % for C13. The annealing heat treatment's increase of mechanical properties can be attributed to two main mechanisms, the increase in PEEK's crystalline phase and the improvement of interfacial adhesion of PEEK prints by increasing molecular diffusion to the printing interfaces. Samples taken from C10 specimens with and without the annealing treatment were submitted to DSC analysis which revealed an increase in the specimen's crystallinity percentage from 33.5 % to 39.15 %. This indicates that high temperature annealing treatments can be used as a post-printing procedure to improve the crystallinity and interfacial adhesion of PEEK prints and thus produce PEEK components with higher strength and stiffness.

4. Conclusions

3D printing parameters were studied for their effects on the tensile and flexural properties of PEEK samples. The parameters of nozzle temperature (NT), zone heater temperature (ZHT), layer height (LH) and extruder multiplier (EM) were selected for their possible influence in the bonding conditions and interfacial adhesion of PEEK prints. Taguchi analysis results for 3D printed PEEK's tensile strength favour the default values of 485 °C for NT, 130 °C for ZHT, 0.2 mm for LH and 1 for EM while the minimum layer height of 0.1 mm is indicated for the tensile modulus. For both the flexural modulus and flexural strength, the optimal parameters from the Taguchi analysis correspond to the maximum values of 495 °C for NT, 150 °C for ZHT, 0.3 mm for LH and 1.1 for the EM. These results are corroborated by the tensile and flexural testing of the samples printed with the optimal parameters which displayed tensile and flexural properties matching the highest values achieved in the DoE study.

In addition to this, different infill configurations were used to produce samples with reductions in void volume of up to 65 % comparatively to non-modified samples which corresponded to increases in both the tensile and flexural properties. For the tensile properties, the alternating infill line angle configuration (C11) produced the highest strength of 89.8 MPa and the highest modulus of 3.82 GPa. Concerning the flexural properties, the best results were achieved with the interlayer line translation infill configurations (C12 and C13) corresponding to a flexural strength of 119.9 MPa for C12 and a flexural modulus of 3.01 GPa for C13. Furthermore, annealing treatments produced further increases of the mechanical properties of the samples with a maximum increase of 29.9 % in tensile modulus and 16.6 % in flexural strength.

Together these results indicate that the mechanical properties of PEEK 3D prints can be increased by focusing on the interfacial adhesion between lines and layers of the print. Improving bond conditions using higher printing temperatures and reducing the samples' void volume by increasing the surfaces of contact between the printed lines. This improvement results in increases in both the strength and stiffness of PEEK 3D prints. For this, the increase of material flow with the extruder multiplier parameter can result in stronger PEEK prints, however, excessive extrusion can also cause flow instability issues and could ultimately damage the printing equipment. Alternatively, different infill configurations can be used to produce denser prints where the contact between lines of different layers is increased. With these configurations, it is possible to achieve significant increases in the strength and stiffness of PEEK 3D prints subject to tensile and flexural loads. Additionally, high-temperature annealing treatments can be used as a post-printing procedure to further increase interfacial adhesion and crystallinity thus resulting in high-performance PEEK 3D printed components.

Declaration of competing interest

The authors declare the following financial interests/personal relationships which may be considered as potential competing interests: B. A. Soares reports financial support was provided by Fundação para a

Ciência e a Tecnologia. Pedro Rendas reports financial support was provided by Fundação para a Ciência e a Tecnologia.

Acknowledgement

The authors acknowledge Fundação para a Ciência e a Tecnologia (FCT, I.P.) for its financial support through the PhD scholarship UI/BD/151082/2021 and through UNIDEMI, project UIDB/00667/2020. The authors would also like to thank João O. Cardoso for the support provided with the DSC analysis equipment.

References

[1] Sachs E, Cima M, Cornie J, Brancazio D, Bredt J, Curodeau A, et al. Three-dimensional printing: the physics and implications of additive manufacturing. CIRP Ann - Manuf Technol 1993;42:257–60. https://doi.org/10.1016/S0007-8506(07)62438-X.
[2] Haryńska A, Carayon I, Kosmela P, Szeliski K, Łapiński M, Pokrywczyńska M, et al. A comprehensive evaluation of flexible FDM/FFF 3D printing filament as a potential material in medical application. Eur Polym J 2020;138:109958. https://doi.org/10.1016/j.eurpolymj.2020.109958.
[3] Garcia J, Yang ZL, Mongrain R, Leask RL, Lachapelle K. 3D printing materials and their use in medical education: a review of current technology and trends for the future. BMJ Simul Technol Enhanc Learn 2018;4:27–40. https://doi.org/10.1136/bmjstel-2017-000234.
[4] Kurtz SM, Devine JN. PEEK biomaterials in trauma, orthopedic, and spinal implants. Biomaterials 2007;28:4845–69. https://doi.org/10.1016/j.biomaterials.2007.07.013.
[5] Kurtz SM. PEEK biomaterials handbook. First Edit. Elsevier; 2012.
[6] Weinans H, Huiskes R, Grootenboer HJ. Effects of material properties of femoral hip components on bone remodeling. J Orthop Res 1992;10:845–53. https://doi.org/10.1002/jor.1100100614.
[7] Berretta S, Evans K, Ghita O. Additive manufacture of PEEK cranial implants: manufacturing considerations versus accuracy and mechanical performance. Mater Des 2018;139:141–52. https://doi.org/10.1016/j.matdes.2017.10.078.
[8] Singh S, Prakash C, Ramakrishna S. 3D printing of polyether-ether-ketone for biomedical applications. Eur Polym J 2019;114:234–48. https://doi.org/10.1016/j.eurpolymj.2019.02.035.
[9] Yang S, Wang L, Chen Q, Xu M. In situ process monitoring and automated multi-parameter evaluation using optical coherence tomography during extrusion-based bioprinting. Addit Manuf 2021;47:102251. https://doi.org/10.1016/j.addma.2021.102251.
[10] Rendas P, Figueiredo L, Machado C, Mourão A, Vidal C, Soares B. Mechanical performance and bioactivation of 3D-printed PEEK for high-performance implant manufacture: a review. Prog Biomater 2022. https://doi.org/10.1007/s40204-022-00214-6.
[11] Naffakh M, Gómez MA, Ellis G, Marco C. Thermal properties, structure and morphology of PEEK/thermotropic liquid crystalline polymer blends. Polym Int 2003;52:1876–86. https://doi.org/10.1002/pi.1276.
[12] Talbott MF, Springer GS, Berglund LA. The effects of crystallinity on the mechanical properties of PEEK polymer and graphite fiber reinforced PEEK. J Compos Mater 1987;21:1056–81. https://doi.org/10.1177/002199838702101104.
[13] Basgul C, Yu T, MacDonald DW, Siskey R, Marcolongo M, Kurtz SM. Does annealing improve the interlayer adhesion and structural integrity of FFF 3D printed PEEK lumbar spinal cages? J Mech Behav Biomed Mater 2020;102:103455. https://doi.org/10.1016/j.jmbbm.2019.103455.
[14] Yang C, Tian X, Li D, Cao Y, Zhao F, Shi C. Influence of thermal processing conditions in 3D printing on the crystallinity and mechanical properties of PEEK material. J Mater Process Technol 2017;248:1–7. https://doi.org/10.1016/j.jmatprotec.2017.04.027.
[15] Wu W, Geng P, Li G, Zhao D, Zhang H, Zhao J. Influence of layer thickness and raster angle on the mechanical properties of 3D-printed PEEK and a comparative mechanical study between PEEK and ABS. Materials (Basel) 2015;8:5834–46. https://doi.org/10.3390/ma8095271.
[16] Pu J, McIlroy C, Jones A, Ashcroft I. Understanding mechanical properties in fused filament fabrication of polyether ether ketone. Addit Manuf 2021;37:101673. https://doi.org/10.1016/j.addma.2020.101673.
[17] Es-Said OS, Foyos J, Noorani R, Mendelson M, Marloth R, Pregger BA. Effect of layer orientation on mechanical properties of rapid prototyped samples. Mater Manuf Process 2000;15:107–22. https://doi.org/10.1080/10426910008912976.
[18] Ahn SH, Montero M, Odell D, Roundy S, Wright PK. Anisotropic material properties of fused deposition modeling ABS. Rapid Prototyp J 2002;8:248–57. https://doi.org/10.1108/13552540210441166.
[19] Masood SH, Mau K, Song WQ. Tensile properties of processed FDM polycarbonate material. Mater Sci Forum 2010;654–656:2556–9. https://doi.org/10.4028/www.scientific.net/MSF.654-656.2556.
[20] Durgun I, Ertan R. Experimental investigation of FDM process for improvement of mechanical properties and production cost. Rapid Prototyp J 2014;20:228–35. https://doi.org/10.1108/RPJ-10-2012-0091.
[21] Rinaldi M, Ghidini T, Cecchini F, Brandao A, Nanni F. Additive layer manufacturing of poly (ether ether ketone) via FDM. Compos Part B Eng 2018;145:162–72. https://doi.org/10.1016/j.compositesb.2018.03.029.
[22] Bellehumeur C, Li L, Sun Q, Gu P. Modeling of bond formation between polymer filaments in the fused deposition modeling process. J Manuf Process 2004;6:170–8. https://doi.org/10.1016/S1526-6125(04)70071-7.
[23] Basgul C, Thieringer FM, Kurtz SM. Heat transfer-based non-isothermal healing model for the interfacial bonding strength of fused filament fabricated polyetheretherketone. Addit Manuf 2021;46:102097. https://doi.org/10.1016/j.addma.2021.102097.
[24] Zhao Y, Zhao K, Li Y, Chen F. Mechanical characterization of biocompatible PEEK by FDM. J Manuf Process 2020;56:28–42. https://doi.org/10.1016/j.jmapro.2020.04.063.
[25] Vaezi M, Yang S. Extrusion-based additive manufacturing of PEEK for biomedical applications. Virtual Phys Prototyp 2015;10:123–35. https://doi.org/10.1080/17452759.2015.1097053.
[26] Wang P, Zou B, Xiao H, Ding S, Huang C. Effects of printing parameters of fused deposition modeling on mechanical properties, surface quality, and microstructure of PEEK. J Mater Process Technol 2019;271:62–74. https://doi.org/10.1016/j.jmatprotec.2019.03.016.
[27] Tseng JW, Liu CY, Yen YK, Belkner J, Bremicker T, Liu BH, et al. Screw extrusion-based additive manufacturing of PEEK. Mater Des 2018;140:209–21. https://doi.org/10.1016/j.matdes.2017.11.032.
[28] Avanzini A, Petrogalli C, Battini D, Donzella G. Influence of micro-notches on the fatigue strength and crack propagation of unfilled and short carbon fiber reinforced PEEK. Mater Des 2018;139:447–56. https://doi.org/10.1016/j.matdes.2017.11.039.
[29] Colmer T, Daniewicz SR, Newman JC, Moser R. Measuring fatigue crack growth and closure in polyether ether ketone (PEEK). Int J Fatigue 2017;95:243–51. https://doi.org/10.1016/j.ijfatigue.2016.10.025.
[30] Deng X, Zeng Z, Peng B, Yan S, Ke W. Mechanical properties optimization of poly-ether-ether-ketone via fused deposition modeling. Materials (Basel) 2018:11. https://doi.org/10.3390/ma11020216.
[31] Mohamed T, Barhoumi N, Lamnawar K, Maazouz A, Znaidi A. Optimization of fused deposition modeling process parameters using the taguchi method to improve the tensile properties of 3D-printed polyether ether ketone. Proc Inst Mech Eng Part L J Mater Des Appl 2021;235:2565–73. https://doi.org/10.1177/14644207211017572.
[32] Wang Y, Müller WD, Rumjahn A, Schmidt F, Schwitalla AD. Mechanical properties of fused filament fabricated PEEK for biomedical applications depending on additive manufacturing parameters. J Mech Behav Biomed Mater 2021;115:104250. https://doi.org/10.1016/j.jmbbm.2020.104250.
[33] Kumar R, Singh G, Chinappan A, Ghomi ER, Singh S, Sandhu K, et al. On mechanical, physical, and bioactivity characteristics of material extrusion printed polyether ether ketone. J Mater Eng Perform 2022. https://doi.org/10.1007/s11665-022-07519-4.
[34] Rodriguez J. In: Maximizing the strength of fused-deposition ABS plastic parts; 1999. p. 335–42. 10th Solid Free …
[35] Rodriguez JF, Thomas JP, Renaud JE. Characterization of the mesostructure of fused-deposition acrylonitrile-butadiene-styrene materials. Rapid Prototyp J 2000;6:175–85. https://doi.org/10.1108/13552540010337056.
[36] Cicala G, Latteri A, Del Curto B, Lo Russo A, Recca G, Farè S. Engineering thermoplastics for additive manufacturing: a critical perspective with experimental evidence to support functional applications. J Appl Biomater Funct Mater 2017;15:e10–8. https://doi.org/10.5301/jabfm.5000343.
[37] Apium PEEK 450 Natural Datasheet. n.d.
[38] Park SJ, Lee JE, Park J, Lee NK, Son Y, Park SH. High-temperature 3D printing of polyetheretherketone products: perspective on industrial manufacturing applications of super engineering plastics. Mater Des 2021;211:110163. https://doi.org/10.1016/j.matdes.2021.110163.
[39] Hu B, Duan X, Xing Z, Xu Z, Du C, Zhou H, et al. Improved design of fused deposition modeling equipment for 3D printing of high-performance PEEK parts. Mech Mater 2019;137:103139. https://doi.org/10.1016/j.mechmat.2019.103139.
[40] Gupta H, Salovey R. Thermal behavior of transparent poly(etheretherketone) (PEEK) film. Polym Eng Sci 1990;30:453–8. https://doi.org/10.1002/pen.760300805.
[41] Regis M, Bellare A, Pascolini T, Bracco P. Characterization of thermally annealed PEEK and CFR-PEEK composites: structure-properties relationships. Polym Degrad Stab 2017;136:121–30. https://doi.org/10.1016/j.polymdegradstab. 2016.12.005.
[42] Bonmatin M, Chabert F, Bernhart G, Djilali T. Rheological and crystallization behaviors of low processing temperature poly(aryl ether ketone). J Appl Polym Sci 2021:138. https://doi.org/10.1002/app.51402.
[43] Blundell DJ, Osborn BN. The morphology of poly(aryl-ether-ether-ketone). Polymer (Guildf) 1983;24:953–8. https://doi.org/10.1016/0032-3861(83)90144-1.
[44] Arevalo SE, Pruitt LA. Nanomechanical analysis of medical grade PEEK and carbon fiber-reinforced PEEK composites. J Mech Behav Biomed Mater 2020;111:104008. https://doi.org/10.1016/j.jmbbm.2020.104008.
[45] Ostberg GMK, Seferis JC. Annealing effects on the crystallinity of polyetheretherketone (PEEK) and its carbon fiber composite. J Appl Polym Sci 1987;33:29–39. https://doi.org/10.1002/app.1987.070330103.
[46] McLauchlin AR, Ghita OR, Savage L. Studies on the reprocessability of poly(ether ether ketone) (PEEK). J Mater Process Technol 2014;214:75–80. https://doi.org/10.1016/j.jmatprotec.2013.07.010.

[47] Arif MF, Kumar S, Varadarajan KM, Cantwell WJ. Performance of biocompatible PEEK processed by fused deposition additive manufacturing. Mater Des 2018;146:249–59. https://doi.org/10.1016/j.matdes.2018.03.015.
[48] Sun Q, Rizvi GM, Bellehumeur CT, Gu P. Effect of processing conditions on the bonding quality of FDM polymer filaments. Rapid Prototyp J 2008;14:72–80. https://doi.org/10.1108/13552540810862028.
[49] Rev T, Xu X, Czél G, Wisnom RM. The effect of transverse compressive stresses on tensile failure of carbon fibre/epoxy composites. Compos Part A Appl Sci Manuf 2022:156.
[50] Kurtz SM. An overview of PEEK biomaterials. In: PEEK Biomater. Handb. 1st Ed. Elsevier Inc.;; 2012. p. 1–7. https://doi.org/10.1016/B978-1-4377-4463-7.10001-6.